HHS Public Access

Author manuscript

J Nucl Med. Author manuscript; available in PMC 2016 April 08.

Published in final edited form as:

J Nucl Med. 2014 July ; 55(7): 1185–1191. doi:10.2967/jnumed.114.138701.

An Improved Antagonist Radiotracer for the Kappa Opioid Receptor: Synthesis and Characterization of ^{11}C-LY2459989

Ming-Qiang Zheng[1], **Su Jin Kim**[1], **Daniel Holden**[1], **Shu-fei Lin**[1], **Anne Need**[2], **Karen Rash**[2], **Vanessa Barth**[2], **Charles Mitch**[2], **Antonio Navarro**[2], **Michael Kapinos**[1], **Kathleen Maloney**[1], **Jim Ropchan**[1], **Richard E. Carson**[1], and **Yiyun Huang**[1,*]

[1]PET Center, Departments of Diagnostic Radiology, Yale University, New Haven, Connecticut, USA

[2]Eli Lilly & Company, Indianapolis, Indiana, USA

Abstract

The kappa opioid receptors (KOR) are implicated in a number of neuropsychiatric diseases and addictive disorders. Positron Emission Tomography (PET) with radioligands provides a means to image the KOR in vivo and investigate its function in health and disease. The purpose of this study was to develop the selective KOR antagonist ^{11}C-LY2459989 as a PET radioligand and characterize its imaging performance in non-human primates.

Methods—LY2459989 was synthesized and assayed for in vitro binding to opioid receptors. Ex vivo studies in rodents were conducted to assess its potential as a tracer candidate. ^{11}C-LY2459989 was synthesized by reaction of its iodophenyl precursor with ^{11}C-cyanide followed by partial hydrolysis of the resulting ^{11}C-cyanophenyl intermediate. Imaging experiments with ^{11}C-LY2459989 were carried out in rhesus monkeys with arterial input function measurement. Imaging data were analyzed with kinetic models to derive in vivo binding parameters.

Results—LY2459989 is a full antagonist with high binding affinity and selectivity for KOR (K_i = 0.18, 7.68, and 91.3 nM, respectively, for κ, μ, and δ receptors). Ex vivo studies in rats indicated LY2459989 as an appropriate tracer candidate with high specific binding signals, and confirmed its KOR binding selectivity in vivo. ^{11}C-LY2459989 was synthesized in high radiochemical purity and good specific activity. In rhesus monkeys, ^{11}C-LY2459989 displayed a fast rate of peripheral metabolism. Similarly, ^{11}C-LY2459989 displayed fast uptake kinetics in the brain and an uptake pattern consistent with the distribution of KOR in primates. Pretreatment with naloxone (1 mg/kg, i.v.) resulted in a uniform distribution of radioactivity in the brain. Further, specific binding of ^{11}C-LY2459989 was dose-dependently reduced by the selective KOR antagonist LY2456302 and the unlabeled LY2459989. Regional binding potential (BP_{ND}) values derived from the multilinear analysis method (MA1), as a measure of in vivo specific binding signal, were 2.18, 1.39, 1.08, 1.04, 1.03, 0.59, 0.51, 0.50, respectively, for the globus pallidus, cingulate cortex, insula, caudate, putamen, frontal cortex, temporal cortex, and thalamus.

*Correspondence Author: Yiyun (Henry) Huang, PET Center, Department of Diagnostic Radiology, Yale University School of Medicine, PO Box 208048, 801 Howard Avenue, New Haven, CT 06520-8048, Telephone: (203)785-3193, Fax: (203)785-2994, henry.huang@yale.edu.

Conclusion—The novel PET radioligand ^{11}C-LY2459989 displayed favorable pharmacokinetic properties, specific and KOR-selective binding profile, and high specific binding signals in vivo, thus making it a promising PET imaging agent for KOR.

Keywords

Kappa opioid receptor; Antagonist; PET; Radioligand; Synthesis and Evaluation

INTRODUCTION

The opioid receptors (ORs) are G-protein–coupled receptors with at least three subtypes: μ, κ and δ (1). The ORs share extensive homology, but differ in their pharmacology and physiological effects (2). Presence of κ-opioid receptors (KOR) is widespread in the human brain, and is found in greater density than the μ-opioid receptor (MOR) in most brain regions (3–5). KOR receptors are present in the deep layers of cortical regions, as well as the striatum, hippocampus, amygdala, and thalamus (3, 5, 6). A similar distribution of KOR is seen in the non-human primate brain (7, 8).

KOR is implicated in the pathophysiology of a variety of neuropsychiatric diseases and addictive disorders (9). For example, multiple lines of evidence point to the involvement of KOR in depression and related mood disorders (10–16). In turn, these findings raise the possibility that KOR antagonists might be efficacious antidepressants. As such, KOR is a target for development of newer antidepressants. In addition, the role of the opioid system in alcohol addiction and treatment is well established, as the non-selective opioid antagonist naltrexone is effective in the prevention of relapse in some alcoholics (17). There is also a large body of literature indicating that the opioid system, especially the KOR, is critically involved in the biology of addiction to psychostimulants and thus pharmacological intervention at the KOR/dynorphin system may be an effective avenue for treatment of drug and alcohol abuse (for a comprehensive review, see (18)).

Since KOR is involved in a number of psychiatric diseases and addictive disorders, the successful deployment of a PET imaging agent for use in humans will allow the non-invasive investigation of KOR in vivo and lead to new understandings of its function and dysfunction/dysregulation in these disorders. It will also make it possible to correlate and translate preclinical findings in animal models to humans and help in the development of novel therapeutic agents by correlating dose, pharmacokinetic parameters, and receptor occupancy.

A number of radiotracers are currently available for imaging the ORs in humans. They include ^{11}C-carfentanil, ^{11}C-/^{18}F-diprenorphine, ^{11}C-buprenorphine, ^{11}C-cyclofoxy, and ^{11}C-methylnaltrindole (for reviews, see (19, 20)). None of these ligands can be used to selectively image KOR in vivo. Over the years, many groups have attempted to develop KOR-selective PET radioligands, such as the agonist ligands ^{11}C-GR89696, ^{11}C-GR103545, and the antagonist ligand ^{11}C-MeJDTic (Figure 1) (21–24). However, only ^{11}C-GR103545 has been evaluated extensively in non-human primates and recently in humans in our laboratory (25–28). We previously reported the synthesis of ^{11}C-LY2795050 as the first ever, selective antagonist radioligand able to image the KOR in non-human primates and humans

(29). In this paper, we report the discovery and characterization of ^{11}C-LY2459989 (^{11}C-**5**, Figure 1) as a KOR-selective radioligand with improved imaging characteristics over ^{11}C-LY2795050.

METERIALS AND METHODS

Chemistry

Synthesis of LY2459989 and the radiolabeling precursor for ^{11}C-LY2459989 is described in the Supplemental Materials.

In Vitro Binding Assays

In vitro binding experiments and GTP-γ-S antagonist functional assays were performed according to the published procedures (30).

Ex Vivo Experiments in Rodents: Tracer Distribution and Receptor Occupancy Studies

Male Sprague-Dawley rats (225–300 g, Harlan Laboratories, Indianapolis, IN) were group-housed with ad libitum food and water and maintained on a 12-hour light/dark cycle. All experiments were conducted under protocols approved by the Institutional Animal Care and Use Committee of Eli Lilly & Company.

LY2459989 was dissolved in 25% 3-hydroxypropyl-β-cyclodextrin at a concentration of 6 μg/mL and administered intravenously via the lateral tail at a dose of 3 μg/kg to groups of rats (4 rats in each group) in a volume of 0.5 mL/kg. Animals were sacrificed at 5, 20, 40, or 60 min after LY2459989 injection. Striatum and cerebellum were dissected, weighed and placed in conical centrifuge tubes placed on ice. Four volumes (w/v) of acetonitrile containing 0.1% formic acid were added to each tube. These samples were then homogenized using an ultrasonic probe (7–8 watts power using sonic probe dismembrator; Fisher Scientific) and centrifuged at 14,000 rpm for 16 min. The supernatant was separated and diluted 1:4 with sterile water in HPLC injection vials for LC/MS/MS analysis using an Agilent model 1200 HPLC (Agilent Technologies, Palo Alto, CA) and an API 4000 mass spectrometer (Applied Biosystems, Foster City, CA, USA). The chromatographic separation employed an Agilent Zorbax Eclipse XDB-C18 column (2.1 × 50 mm, 3.5 μm) and a mobile phase gradient of acetonitrile (A) and water (B), each containing 0.1% formic acid over 5 min (5% A for 1 min, then increasing to 95% A from 1 to 2 min and holding from 2 to 3 min, decreasing to 5% A at 3.1 min and holding until 5 min), at a flow rate of 0.25 mL/min. Detection of LY2459989 was accomplished by monitoring the precursor to product ion transition with a mass to charge ratio (m/z) of 392.301 to 244. Standards were prepared by adding known quantities of LY2459989 to brain tissue samples from non-treated rats and processed as described above. Concentrations of LY2459989 in the striatum were presumed to represent total binding, while levels in the cerebellum represented non-specific binding as this is a region with little or no expression of opioid receptors (31). The concentration ratio between striatum and cerebellum is presented as a measure of specific binding.

Occupancies of LY2459989 at KOR, MOR, and DOR were determined utilizing an in vivo rat model of central receptor occupancy (RO) and the procedures described previously, with

GR103545, naltrexone, and naltriben as in vivo tracers for KOR, MOR, and DOR, respectively (32). They were injected intravenously 1 h after oral administration of vehicle or LY2459989 (0.01, 0.03. 0.1, 0.3, 1, 3, 10, or 30 mg/kg). Animals were sacrificed by cervical dislocation 30 min after tracer administration. Tracer analysis was carried out using an Agilent model 6460 MS/MS equipped with a 1260 HPLC system (Agilent Technologies, Palo Alto, CA). The chromatographic separation was performed with an Agilent Zorbax SB-C18 column (2.1 × 50 mm, 1.8 μm) and gradient of components A (0.1% formic acid in acetonitrile) and B (0.1% formic acid in water) over 3.5 min (5% A for 1 min, then increasing to 90% A from 1 to 1.75 min and holding from 1.75 to 2 min, decreasing to 5% A at 2.1 min and holding until 3.5 min) at a flow rate of 0.40 mL/min. Detection of tracers was accomplished by monitoring ion transitions 414.1/343.0, 342.2/270.2, and 416.0/301.1 mass/charge ratio for GR103545, naltrexone, and naltriben, respectively.

Radiochemistry

Instruments used were as follows: a preparative HPLC system including a Shimadzu LC-20A pump, a Rheodyne 7133i injector with a 2 mL loop, a Knauer K200 UV detector, a Bioscan gamma flow detector, and a laptop PC running the EZStart data acquisition software; an analytical HPLC system consisting of a Shimadzu LC-20A quarternary pump, a Rheodyne 7133i injector, a Shimadzu SPD-M20A PDA or SPD-20A UV detector, a flow cell gamma detector (Bioscan) and a PC with Shimadzu Class VP 7.2 software used for system control. Chiral HPLC analysis was performed with a Chiralpak AS-H column (4.6 × 150 mm) eluting with 0.2% triethylamine in MeOH at a flow rate of 0.6 mL/min.

Production of ^{11}C-CO_2 was started with the ^{14}N(p,α)^{11}C nuclear reaction by bombarding with a proton source a mixture of nitrogen with oxygen (0.5–1%) in a high pressure target in a GE PETtrace cyclotron. The cyclotron produced ^{11}C-CO_2 was transferred into a GE ProCab and reacted with hydrogen at 400 °C under a nickel catalyst to afford ^{11}C-methane, which was converted to ^{11}C-cyanide by reaction with ammonia over a platinum catalyst at 950 °C. Radiolabeling was performed by trapping ^{11}C-cyanide in a solution of precursor **6** (1–3 mg) (Figure 3), K_2HCO_3, Pd_2dba_3 and dppf in DMF (0.3 mL) at room temperature, and then reacted at 80 °C for 5 min to produce the intermediate ^{11}C-**7**, which was then treated with NaOH (1 N, 0.2 mL) and H_2O_2 (0.2 mL) at 80 °C for 5 min to afford ^{11}C-LY2459989 (^{11}C-**5**) (Figure 3).

Purification was achieved by preparative HPLC using a Genesis C18 column (10 × 250 mm, 4 μm). The column was eluted with 22% acetonitrile and 78% 0.1 M aqueous ammonium formate solution with 0.5% acetic acid (v/v, pH 4.2), at a flow rate of 5 mL/min. The desired product fraction (eluting at 11 to 13 min) was collected, diluted with water (50 mL), and passed through a Waters C-18 SepPak cartridge. The catridge was rinsed with 10 mL of 0.01N HCl solution. The radioactive product was recovered by eluting the SepPak with 1 mL of USP absolute ethanol, followed by 3 mL of USP saline, into a product vial containing 7 mL of USP saline and 40 μL of 4.2% USP sodium bicarbonate solution. This mixture was then passed through a sterile membrane filter (0.22 μm) for terminal sterilization and collected in an empty sterile vial to afford a formulated solution ready for intravenous administration. Chemical purity, radiochemical purity, and specific activity of ^{11}C-

LY2459989 were determined by HPLC analysis of the final product solution (column: Genesis C18, 4.6 × 250 mm, 4 μm; mobile phase: 22% acetonitrile and 78% 0.1 M aqueous ammonium formate with 0.5% acetic acid (v/v, pH 4.2); flow rate: 2 mL/min; UV detector wavelength: 254 nm). Identity of the labeled compound was confirmed by co-injection of the product with the unlabeled LY2459989. Radiolabeled product and LY2459989 co-eluted on the analytical HPLC (Retention time for the product: ~6.3 min).

PET Imaging Experiments in Rhesus Monkeys

PET Procedures—Experiments were performed in rhesus monkeys (macaca mulatta) according to a protocol approved by the Yale University Institutional Animal Care and Use Committee (IACUC) and procedures as described previously (33).

Three animals were used in this study. In the first set of experiments, a control scan with [^{11}C]LY2459989 alone was followed by a blocking scan with i.v. injection of naloxone (1 mg/kg) at 10 min before the second injection of [^{11}C]LY2459989. In the second set of experiments, a [^{11}C]LY2459989 baseline scan was followed by a blocking scan either with LY2456302 (29, 30), or the unlabeled LY2459989. A total of 12 PET scans were performed.

Metabolite Analysis and Arterial Input Function Measurement—Procedures for measurement of the input function have previously been described (29). Arterial samples were collected at pre-selected time points to measure radioactivity concentration in plasma and whole blood. Six samples, collected at 5, 15, 30, 60, and 90 min, were also processed and analyzed by HPLC to determine the fraction of unmetabolized tracer over time using a column-switching method (34). Procedures for sample preparation, HPLC analysis and data processing were the same as those previously reported for ^{11}C-LY2795050 (29). Procedure for plasma free fraction (f_p) measurement was also the same.

Image Analysis and Kinetic Modeling—Procedures for PET image reconstruction and definition of regions-of-interest (ROI) were the same as described previously (29). For each scan, radiotracer concentrations over time were measured in 15 ROIs.

Total distribution volume (V_T, mL·cm^{-3}) was derived by kinetic analysis of the regional time–activity curves (TACs), using the metabolite-corrected arterial plasma concentration as the input function, according to a 1-tissue (1T) or 2-tissue (2T) compartment model, as well as the multilinear analysis-1 (MA1) method (35, 36). Kinetic parameters (K_1 and k_2 for the 1T model; K_1–k_4 for the 2T model) were derived first. In the 1T model, K_1 (mL·min^{-1}·cm^{-3}) and k_2 (min^{-1}) are the rate constants governing the transfer of the ligand into and out of the brain, respectively. In the 2T model, K_1 and k_2 are the rate constants governing the transfer of the ligand into and out of the nondisplaceable compartment, whereas k_3 (min^{-1}) and k_4 (min^{-1}) describe the respective rates of association to and dissociation from the receptors (36). Values of V_T were calculated from the kinetic parameters as K_1/k_2 in the 1T model, and as $(K_1/k_2)*(1 + k_3/k_4)$ in the 2T model (36). The Akaike Information Criterion (AIC) was used to evaluate the optimal model for regional V_T estimates.

Cerebellar V_T ($V_{T\ CER}$) was used as an estimate of the nondisplaceable distribution volume to calculate the regional non-displaceable binding potential (BP_{ND}), as $BP_{ND} = (V_{T\ ROI} - V_{T\ CER})/V_{T\ CER}$ (36).

KOR occupancies by naloxone, LY2456302 or LY2459989 were calculated using V_T values from all 15 ROIs to create occupancy plots according to the method of Cunningham et al. (37).

RESULTS

Chemistry

Both LY2459989 (**5**, Figure 1) and its less active (*R*)-enantiomer were synthesized in 98% enantiomeric purity. The radiolabeling precursor (**6**, Figure 2) was also prepared in >99% chemical purity, and >99% enantiomeric purity. Detailed synthetic procedures are described in the Supplemental Material.

In vitro binding assays and ex vivo evaluation in rats

LY2459989 displayed high KOR affinity (K_i = 0.18 nM) and over 43-fold selectivity for KOR over other opioid receptors (K_i = 7.68 nM for MOR and 91.3 nM for DOR) (Supplemental Materials).

The potential of LY2459989 as a tracer candidate was assessed in rats using a 3 μg/kg intravenous dose and analysis of tissue concentrations by LC/MS/MS method (38). A rapid initial brain uptake was seen at 5 min post-injection. Ligand concentration was higher in striatum than cerebellum at all time points (Figure 2A). Striatum to cerebellum concentration ratio, as a measure of specific binding, was 2.9, 4.1, and 4.0, respectively, at 20, 40, and 60 min post-injection.

In vivo binding at KOR, MOR and DOR was also assessed with LC/MS/MS after oral administration of ascending doses of LY2459989 using the triple tracer method (32). Dose dependent blockade of KOR and MOR binding by LY2459989 was demonstrated, resulting in an ED_{50} of 0.31 mg/kg and 19.5 mg/kg, respectively, for KOR and MOR (Figure 2B). These ED_{50} values translated to a selectivity of ~63 folds for KOR over MOR, similar to the selectivity measured in vitro (~43 times, Supplemental Material, Table S1). At the maximum dose administered (30 mg/kg), LY2459989 induced no blockade of DOR binding, consistent with its low affinity for this receptor subtype (Figure 2B and Supplemental Material, Table S1).

Radiochemistry

Radiosynthesis of ^{11}C-LY2459989 is depicted in Figure 3. Palladium-catalyzed displacement of the iodo group in the precursor by ^{11}C-cyanide resulted in the intermediate ^{11}C-**7**, which, without separation and purification, was reacted with H_2O_2 under basic condition to afford the amide ^{11}C-LY2459989 (^{11}C-**5**). This two-step one-pot radiosynthesis provided ^{11}C-LY2459989 in >99% enantiomeric purity (Figure 4). Radiochemical purity of the product was >98%. Radiochemical yield was 7.4 ± 3.8% at the end of synthesis (EOS, calculated from trapped ^{11}C-cyanide and uncorrected for decay),

with specific activity of 22.6 ± 0.9 GBq/μmol (EOS, n = 16). Total synthesis time was 40 ± 5 min.

In vivo evaluation in rhesus monkeys

Following a bolus injection of ^{11}C-LY2459989 (140.6 ± 45.5 MBq, specific activity of 12.2 ± 4.7 GBq/μmol at time of injection, and injected mass of 4.8 ± 0.7 μg, n = 12) into a rhesus monkey, total activity and parent activity in the plasma exhibited a rapid rise and clearance phase, and then either stabilized or decreased slowly over time (Figure 5A). At 30 min after tracer injection, parent fraction was ~25%, indicating a fairly rapid metabolism of the radioligand (Figure 5B). The plasma free fraction of ^{11}C-LY2459989 was about 4.6%, compared to less than 1% for ^{11}C-LY2795050 (29).

In the rhesus monkey brain, ^{11}C-LY2459989 displayed good uptake and a heterogeneous distribution pattern (Figure 6A). The non-selective opioid antagonist naloxone at a dose of 1 mg/kg reduced ^{11}C-LY2459989 uptake in all brain regions to nearly homogeneous levels (Figure 6B), an effect similarly induced by 0.3 mg/kg of the selective kappa antagonist LY2456302 (Figure 6C).

Time activity curves (TACs) of ^{11}C-LY2459989 in selected brain regions are presented in Figure 7. Higher uptake was seen in the globus pallidus, cingulate cortex, insula, caudate, and putamen, lower in the frontal cortex and thalamus, and lowest in the cerebellum (Figure 7A). Regional activity in the brain typically reached peak levels within 10–20 min after tracer injection, indicating fast uptake kinetics. When naloxone was given before ^{11}C-LY2459989, TACs in higher binding regions trended down to the same level as that in the cerebellum (Figure 7B). Furthermore, regional uptake of ^{11}C-LY2459989 was also markedly reduced by pretreatment with LY2456302 (0.3 mg/kg, Figure 7C) and the unlabeled LY2459989 (36 μg/kg, Figure 7D).

Regional TACs were analyzed with 1T and 2T compartment models (36), as well as the MA1 method (35) using the metabolite-corrected plasma input function. The 2T model was found to provide better fits to the data than the 1T model [AIC (2T) < AIC (1T)]. Therefore, 2T would be considered an appropriate model for analysis of the imaging data. Regional V_T values (mL·cm^{-3}) estimated by MA1 showed high correlation with 2T values ($V_{T\,(MA1)} = 0.987\,V_{T\,(2T)} + 0.027$, $r^2 = 0.994$). Listed in Table 1 are MA1-derived V_T values. Regional values of non-displaceable binding potential (BP_{ND}), as a measure of specific binding signal, were calculated using cerebellum as the reference region (Table 1). In the baseline scans, MA1-derived V_T or BP_{ND} values followed the order of globus pallidus > cingulate cortex > insula ~ caudate ~ putamen > frontal cortex ~ temporal cortex ~ thalamus > cerebellum. When the monkeys were pre-treated with naloxone (1 mg/kg), LY2456302 (0.3 mg/kg), or unlabeled LY2459989 (36 μg/kg), specific binding of ^{11}C-LY2459989 was significantly blocked, as reflected by the negligible BP_{ND} values in most brain regions. Based on occupancy plot analysis of the MA1-derived V_T values (37), 91 ± 2% of KOR was occupied by 1 mg/kg of naloxone in two monkeys. KOR occupancies of 77 and 93%, respectively, were induced by 0.03 and 0.3 mg/kg of LY2456302, while occupancy of 72 ± 5% was achieved in the self-blocking experiments with 36 μg/kg of LY2459989 in two separate monkeys.

DISCUSSION

In this paper we describes the synthesis and evaluation of ^{11}C-LY2459989 as an improved antagonist radiotracer for PET imaging of kappa opioid receptor (KOR) in rhesus monkeys. ^{11}C-LY2459989 is a fluorine-containing analog of ^{11}C-LY2795050, a first antagonist tracer developed at our laboratory and shown to be suitable for in vivo imaging and quantification of KOR in non-human primates (29). LY2459989 was synthesized in a route similar to that for LY2795050 (30). In radioligand competition assays in vitro, LY2459989 displayed high KOR binding affinity (K_i = 0.18 nM) and more than 43-fold selectivity for KOR over other opioid receptors (K_i = 7.68 nM for MOR and 91.3 nM for DOR). Compared with LY2795050 (K_i = 0.72 nM for KOR), LY2459989 exhibited 4 times higher KOR affinity and similar selectivity. Given this favorable in vitro binding profile, ex vivo evaluation was carried out in rodents to assess its potential as a tracer candidate.

LY2459989 was administered intravenously to rats at a dose of 3 μg/kg. This dose was selected to be low enough to approximate tracer conditions and at the meanwhile allow accurate measurement of tissue concentrations by LC/MS/MS analysis (32). LY2459989 was found to have excellent brain penetration, with initial uptake levels of 24.7 and 14.4 ng/g in the striatum and cerebellum at 5 min post-injection, which were more than 6 times higher than those of LY2795050 (4.0 and 2.0 ng/g) (29). Specific binding of LY2459989 was also higher, with striatum to cerebellum ratios of 4.1 and 4.0 at 40 and 60 min post-injection, respectively, vs. 2.2 and 3.3 for LY2795050 (29).

Receptor occupancies at the rat KOR, MOR and DOR were also assessed with LC/MS/MS after oral administration of ascending doses of LY2459989 using the triple tracer method, with intravenous injection of GR103545 (1.5 μg/kg), naltrexone (10 μg/kg), and naltriben (10 μg/kg) as tracers for measuring binding to KOR, MOR and DOR (32). KOR and MOR binding was reduced by LY2459989 in a dose-dependent manner. From the saturation curves LY2459989 ED_{50} was calculated to be 0.31 mg/kg for KOR and 19.5 mg/kg for MOR, which corresponded to ~63-fold KOR/MOR selectivity in vivo, consistent with the ~43 times KOR/MOR selectivity measured in vitro.

The radiolabeled ligand ^{11}C-LY2459989 was prepared in high radiochemical purity in a two-step radiosynthetic pathway using ^{11}C-HCN as the radiolabeling agent. The reaction conditions used in the radiosynthesis did not lead to any racemization of the chiral structure, and thus resulted in high enantiomeric purity (>99%) of the product.

PET imaging experiments in rhesus monkeys indicated a fairly rapid rate of metabolism for ^{11}C-LY2459989, with ~25% of parent tracer remaining in the plasma at 30 min post-injection. Similarly, fast uptake kinetics was detected in the monkey brain, with peak uptake times within 10–20 min after tracer administration. Distribution of ^{11}C-LY2459989 was consistent with the rank order of KOR concentrations in monkey brain regions. Regional time-activity curves were amenable to kinetic analysis by 2T model and the MA1 method to derive reliable estimates of binding parameters (V_T and BP_{ND}). In blocking experiments, binding of ^{11}C-LY2459989 in KOR-rich regions was significantly reduced by pretreatment of the monkeys with either the non-selective opioid receptor antagonist naloxone (1 mg/kg),

or the unlabeled LY2459989 (36 μg/kg). Further, pretreatment with the selective KOR antagonist LY2456302 decreased ^{11}C-LY2459989 binding in a dose-dependent manner. Further, V_T remained largely unchanged in the cerebellum when various blocking drugs were administered, suggesting that, in the rhesus monkey, the cerebellum could be used as a reference region. As a measure of specific binding signals, BP_{ND} was calculated from MA1-derived V_T using cerebellum as the reference region. Values of BP_{ND} were high, and >0.5 in most brain regions, and thus can be reliably measured from kinetic analysis of PET imaging data (Table 1) (39). Taken together, results from the current study demonstrated several favorable characteristics of ^{11}C-LY2459989 as a PET imaging tracer, such as fast uptake kinetic, specific and selective binding to KOR, and high specific binding signals in vivo.

Compared with ^{11}C-LY2795050, the new PET radioligand ^{11}C-LY2459989 displays higher *in vitro* binding affinity for KOR with similar selectivity over other opioid receptors. In rhesus monkeys, both tracers display good brain uptake (peak SUV of ~3) and fast tissue kinetics with peak uptake levels within 10–20 min post-injection. Owing to the higher KOR binding affinity, specific binding of ^{11}C-LY2459989 is much higher, with regional BP_{ND} values more than twice of those for ^{11}C-LY2795050 in the monkey brain (Table 1).

CONCLUSION

In this report we demonstrate that the novel radioligand ^{11}C-LY2459989 exhibits a favorable metabolic profile, brain uptake kinetics appropriate for a C-11 tracer, and high regional specific binding signals in rhesus monkeys. Hence, ^{11}C-LY2459989 represents a much improved radiotracer for PET imaging and quantification of KOR in vivo.

Supplementary Material

Refer to Web version on PubMed Central for supplementary material.

Acknowledgments

The authors wish to thank the staff at the Yale PET Center for their expert technical assistance. The study was supported by a grant from the National Institute of Mental Health (R21MH092664). This publication was also made possible by CTSA Grant Number UL1 RR024139 from the National Center for Research Resources (NCRR) and the National Center for Advancing Translational Science (NCATS), components of the National Institutes of Health (NIH), and NIH roadmap for Medical Research. Its contents are solely the responsibility of the authors and do not necessarily represent the official view of NIH.

References

1. Dhawan BN, Cesselin F, Raghubir R, et al. International Union of Pharmacology. XII. Classification of opioid receptors. Pharmacol Rev. 1996; 48:567–592. [PubMed: 8981566]
2. Minami M, Satoh M. Molecular biology of the opioid receptors: structures, functions and distributions. Neurosci Res. 1995; 23:121–145. [PubMed: 8532211]
3. Hiller JM, Fan LQ. Laminar distribution of the multiple opioid receptors in the human cerebral cortex. Neurochem Res. 1996; 21:1333–1345. [PubMed: 8947923]
4. Mathieu-Kia AM, Fan LQ, Kreek MJ, Simon EJ, Hiller JM. μ-, δ- and κ-opioid receptor populations are differentially altered in distinct areas of postmortem brains of Alzheimer's disease patients. Brain Res. 2001; 893:121–134. [PubMed: 11223000]

5. Peckys D, Landwehrmeyer GB. Expression of mu, kappa, and delta opioid receptor messenger RNA in the human CNS: a ^{33}P in situ hybridization study. Neuroscience. 1999; 88:1093–1135. [PubMed: 10336124]
6. Simonin F, Gaveriaux-Ruff C, Befort K, et al. κ-Opioid receptor in humans: cDNA and genomic cloning, chromosomal assignment, functional expression, pharmacology, and expression pattern in the central nervous system. Proc Natl Acad Sci U S A. 1995; 92:7006–7010. [PubMed: 7624359]
7. Ko MC, Lee H, Harrison C, et al. Studies of μ-, κ-, and δ-opioid receptor density and G protein activation in the cortex and thalamus of monkeys. J Pharmacol Exp Ther. 2003; 306:179–186. [PubMed: 12676881]
8. Slater P, Cross AJ. Autoradiographic distribution of dynorphin1–9 binding sites in primate brain. Neuropeptides. 1986; 8:71–76. [PubMed: 2876397]
9. Tejeda HA, Shippenberg TS, Henriksen R. The dynorphin/κ-opioid receptor system and its role in psychiatric disorders. Cell Mol Life Sci. 2012; 69:857–896. [PubMed: 22002579]
10. McLaughlin JP, Marton-Popovici M, Chavkin C. Kappa opioid receptor antagonism and prodynorphin gene disruption block stress-induced behavioral responses. J Neurosci. 2003; 23:5674–5683. [PubMed: 12843270]
11. Newton SS, Thome J, Wallace TL, et al. Inhibition of cAMP response element-binding protein or dynorphin in the nucleus accumbens produces an antidepressant-like effect. J Neurosci. 2002; 22:10883–10890. [PubMed: 12486182]
12. Shirayama Y, Ishida H, Iwata M, Hazama GI, Kawahara R, Duman RS. Stress increases dynorphin immunoreactivity in limbic brain regions and dynorphin antagonism produces antidepressant-like effects. J Neurochem. 2004; 90:1258–1268. [PubMed: 15312181]
13. Carlezon WA Jr, Beguin C, DiNieri JA, et al. Depressive-like effects of the kappa-opioid receptor agonist salvinorin A on behavior and neurochemistry in rats. J Pharmacol Exp Ther. 2006; 316:440–447. [PubMed: 16223871]
14. Beardsley PM, Howard JL, Shelton KL, Carroll FI. Differential effects of the novel kappa opioid receptor antagonist, JDTic, on reinstatement of cocaine-seeking induced by footshock stressors vs cocaine primes and its antidepressant-like effects in rats. Psychopharmacology (Berl). 2005; 183:118–126. [PubMed: 16184376]
15. Mague SD, Pliakas AM, Todtenkopf MS, et al. Antidepressant-like effects of kappa-opioid receptor antagonists in the forced swim test in rats. J Pharmacol Exp Ther. 2003; 305:323–330. [PubMed: 12649385]
16. Reindl JD, Rowan K, Carey AN, Peng X, Neumeyer JL, McLaughlin JP. Antidepressant-like effects of the novel kappa opioid antagonist MCL-144B in the forced-swim test. Pharmacology. 2008; 81:229–235. [PubMed: 18176093]
17. O'Malley SS, Froehlich JC. Advances in the use of naltrexone: an integration of preclinical and clinical findings. Recent Dev Alcohol. 2003; 16:217–245. [PubMed: 12638640]
18. Shippenberg TS, Zapata A, Chefer VI. Dynorphin and the pathophysiology of drug addiction. Pharmacol Ther. 2007; 116:306–321. [PubMed: 17868902]
19. Henriksen G, Willoch F. Imaging of opioid receptors in the central nervous system. Brain. 2008; 131:1171–1196. [PubMed: 18048446]
20. Dannals RF. Positron emission tomography radioligands for the opioid system. J Labelled Compd Radiopharm. 2013; 56:187–195.
21. Chesis PL, Welch MJ. Synthesis and in vitro characterization of fluorinated U-50488 analogs for PET studies of kappa opioid receptors. Int J Rad Appl Instrum [A]. 1990; 41:267–273.
22. Noble G, Dannals RF, Ravert HT, Wilson AA, Wagner HN. Synthesis of a radiotracer for studying k-subtype opiate receptors: *N*-[^{11}C-methyl]-*N*-(trans-2-pyrrolidinyl-cyclohexyl)-3,4-dichlorophenylacetamide ([^{11}C]-(±)-U-50488H). J Labelled Compd Radiopharm. 1992; 31:81–89.
23. Ravert HT, Mathews WB, Musachio JL, Scheffel U, Finley P, Dannals RF. [^{11}C]-Methyl 4-[(3,4-dichlorophenyl)acetyl]-3-[(1-pyrrolidinyl)-methyl]-1-piperazinecarboxylate ([^{11}C]GR89696): synthesis and in vivo binding to kappa opiate receptors. Nucl Med Biol. 1999; 26:737–741. [PubMed: 10628552]

24. Ravert HT, Scheffel U, Mathews WB, Musachio JL, Dannals RF. [^{11}C]-GR89696, a potent kappa opiate receptor radioligand; in vivo binding of the R and S enantiomers. Nucl Med Biol. 2002; 29:47–53. [PubMed: 11786275]
25. Tomasi G, Nabulsi N, Zheng MQ, et al. Determination of in vivo B_{max} and K_d for ^{11}C-GR103545, an agonist PET tracer for kappa-opioid receptors: a study in nonhuman primates. J Nucl Med. 2013; 54:600–608. [PubMed: 23424192]
26. Talbot PS, Narendran R, Butelman ER, et al. ^{11}C-GR103545, a radiotracer for imaging kappa-opioid receptors in vivo with PET: Synthesis and evaluation in baboons. J Nucl Med. 2005; 46:484–494. [PubMed: 15750163]
27. Schoultz BW, Hjornevik T, Willoch F, et al. Evaluation of the kappa-opioid receptor-selective tracer [^{11}C]GR103545 in awake rhesus macaques. Eur J Nucl Med Mol Imaging. 2010; 37:1174–1180. [PubMed: 20157708]
28. Poisnel G, Oueslati F, Dhilly M, et al. [^{11}C]-MeJDTic: a novel radioligand for kappa-opioid receptor positron emission tomography imaging. Nucl Med Biol. 2008; 35:561–569. [PubMed: 18589300]
29. Zheng MQ, Nabulsi N, Kim SJ, et al. Synthesis and evaluation of ^{11}C-LY2795050 as a kappa-opioid receptor antagonist radiotracer for PET imaging. J Nucl Med. 2013; 54:455–463. [PubMed: 23353688]
30. Mitch CH, Quimby SJ, Diaz N, et al. Discovery of aminobenzyloxyarylamides as kappa opioid receptor selective antagonists: application to preclinical development of a kappa opioid receptor antagonist receptor occupancy tracer. J Med Chem. 2011; 54:8000–8012. [PubMed: 21958337]
31. Mansour A, Fox CA, Burke S, et al. Mu, delta, and kappa opioid receptor mRNA expression in the rat CNS: an in situ hybridization study. J Comp Neurol. 1994; 350:412–438. [PubMed: 7884049]
32. Need AB, McKinzie JH, Mitch CH, Statnick MA, Phebus LA. In vivo rat brain opioid receptor binding of LY255582 assessed with a novel method using LC/MS/MS and the administration of three tracers simultaneously. Life Sci. 2007; 81:1389–1396. [PubMed: 17935738]
33. Nabulsi N, Huang Y, Weinzimmer D, et al. High-resolution imaging of brain 5-HT$_{1B}$ receptors in the rhesus monkey using [^{11}C]P943. Nucl Med Biol. 2010; 37:205–214. [PubMed: 20152720]
34. Hilton J, Yokoi F, Dannals RF, Ravert HT, Szabo Z, Wong DF. Column-switching HPLC for the analysis of plasma in PET imaging studies. Nucl Med Biol. 2000; 27:627–630. [PubMed: 11056380]
35. Ichise M, Toyama H, Innis RB, Carson RE. Strategies to improve neuroreceptor parameter estimation by linear regression analysis. J Cereb Blood Flow Metab. 2002; 22:1271–1281. [PubMed: 12368666]
36. Innis RB, Cunningham VJ, Delforge J, et al. Consensus nomenclature for in vivo imaging of reversibly binding radioligands. J Cereb Blood Flow Metab. 2007; 27:1533–1539. [PubMed: 17519979]
37. Cunningham VJ, Rabiner EA, Slifstein M, Laruelle M, Gunn RN. Measuring drug occupancy in the absence of a reference region: the Lassen plot re-visited. J Cereb Blood Flow Metab. 2010; 30:46–50. [PubMed: 19738632]
38. Chernet E, Martin LJ, Li D, et al. Use of LC/MS to assess brain tracer distribution in preclinical, in vivo receptor occupancy studies: Dopamine D$_2$, serotonin 2A and NK-1 receptors as examples. Life Sci. 2005; 78:340–346. [PubMed: 16139310]
39. Laruelle M, Slifstein M, Huang Y. Relationships between radiotracer properties and image quality in molecular imaging of the brain with positron emission tomography. Mol Imaging Biol. 2003; 5:363–375. [PubMed: 14667491]

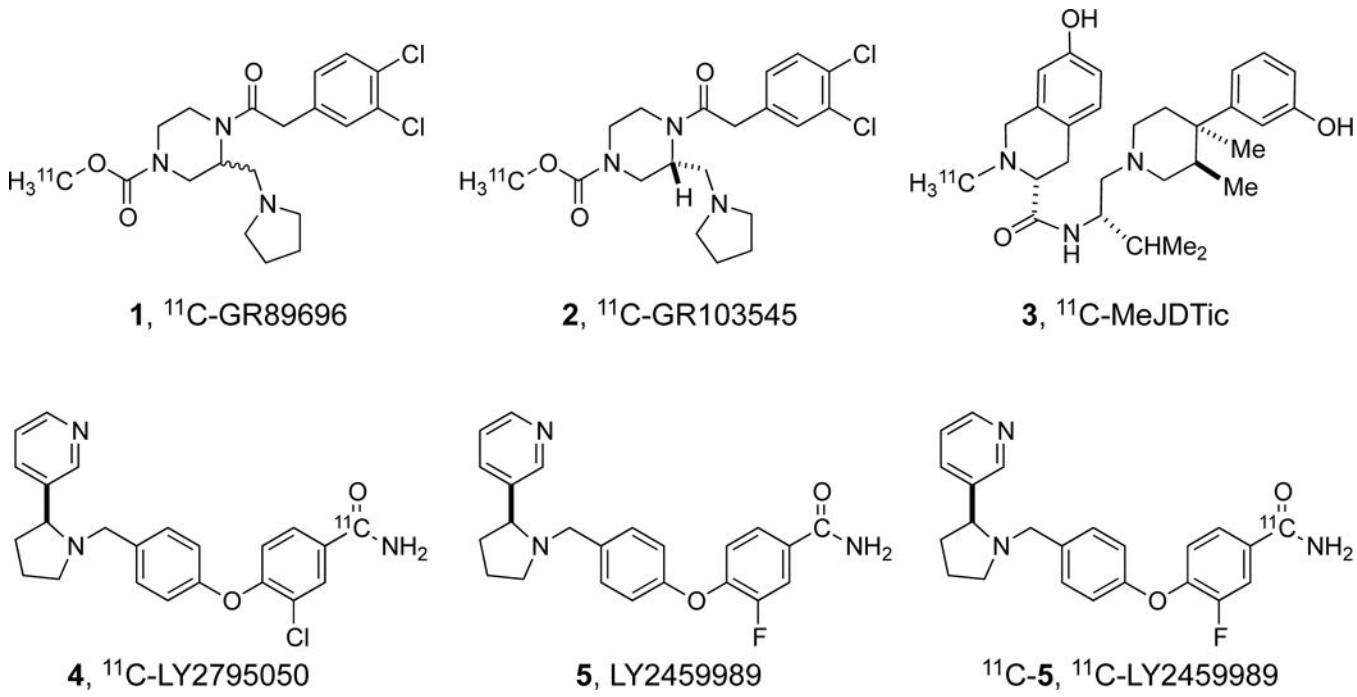

Figure 1.
Structures of selected kappa opioid receptor ligands.

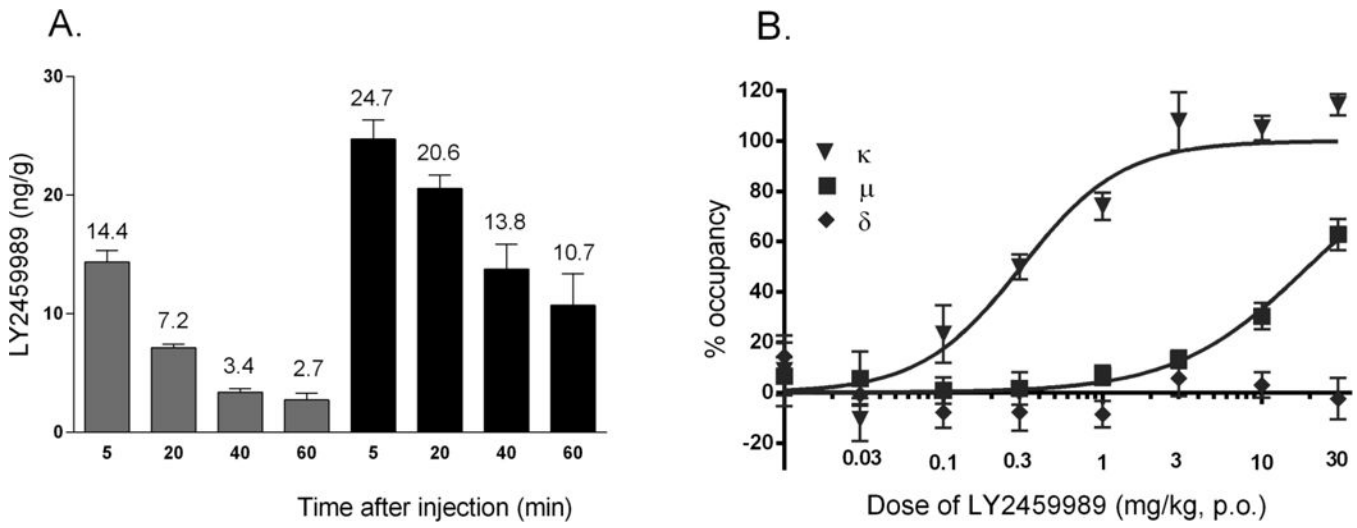

Figure 2.

A: Ligand concentrations (ng/g of brain tissue) in the cerebellum (grey bar) and striatum (black bar) of Sprague-Dawley rats at 5, 20, 40 and 60 min (n = 4 rats per time point) following intravenous administration of LY2459989 (3 μg/g); B: Dose-receptor occupancy relationship of LY2459989 at KOR, MOR and DOR.

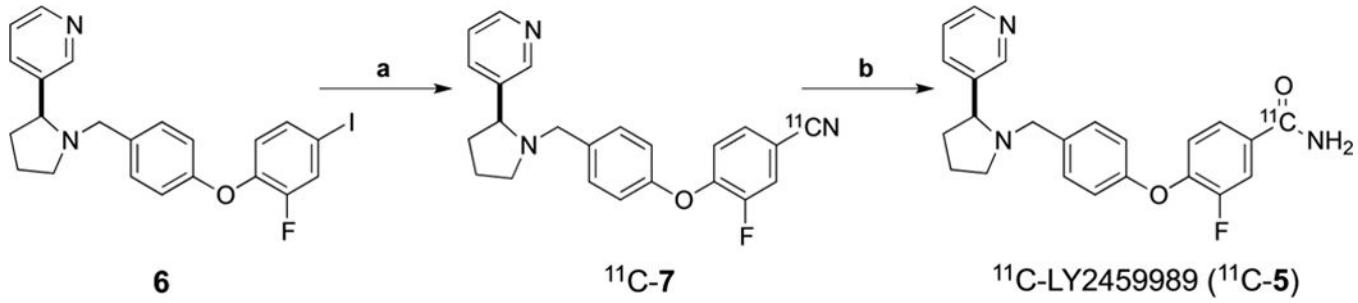

Figure 3.

Radiosynthesis of ^{11}C-LY2459989.

Reagents and conditions: **a**. H^{11}CN, $KHCO_3$, dppf, Pd_2dba_3, DMF, 80 °C, 5 min; **b**. NaOH, H_2O_2, 80 °C, 5 min.

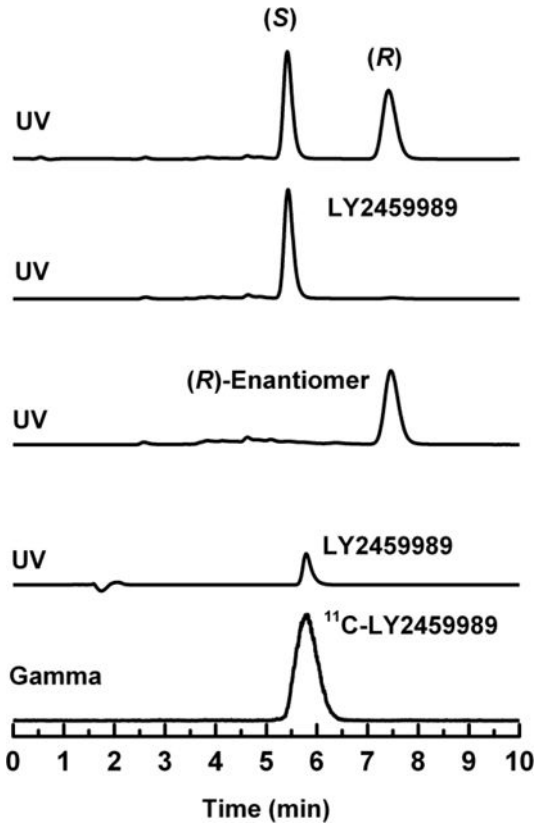

Figure 4.

Chiral HPLC chromatograms for the racemic compound (first row), the (*S*)-enantiomer LY2459989 (second row), the (*R*)-enantiomer (third row) and the radiolabeled compound ^{11}C-LY2459989 (last two rows). The (*S*)-enantiomer eluted first at 5.4 min, and the (*R*)-enantiomer eluted later at 7.5 min.

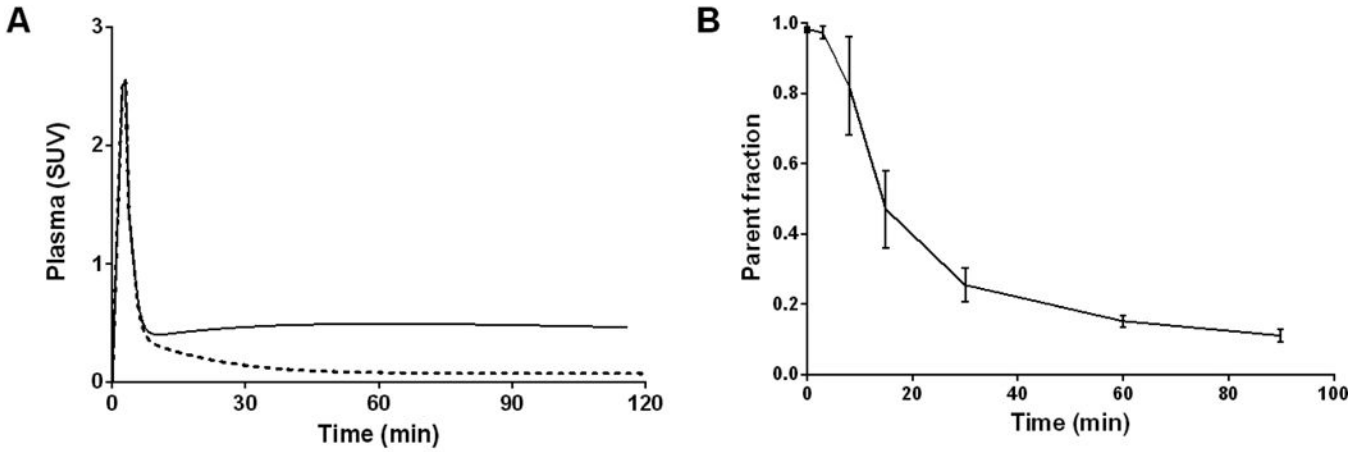

Figure 5.

Analysis of ^{11}C-LY2459989 in the plasma: A. Total radioactivity (solid line) and metabolite-corrected parent activity (dotted line) over time; B. Time course of parent fraction from six baseline scans (mean ± SD).

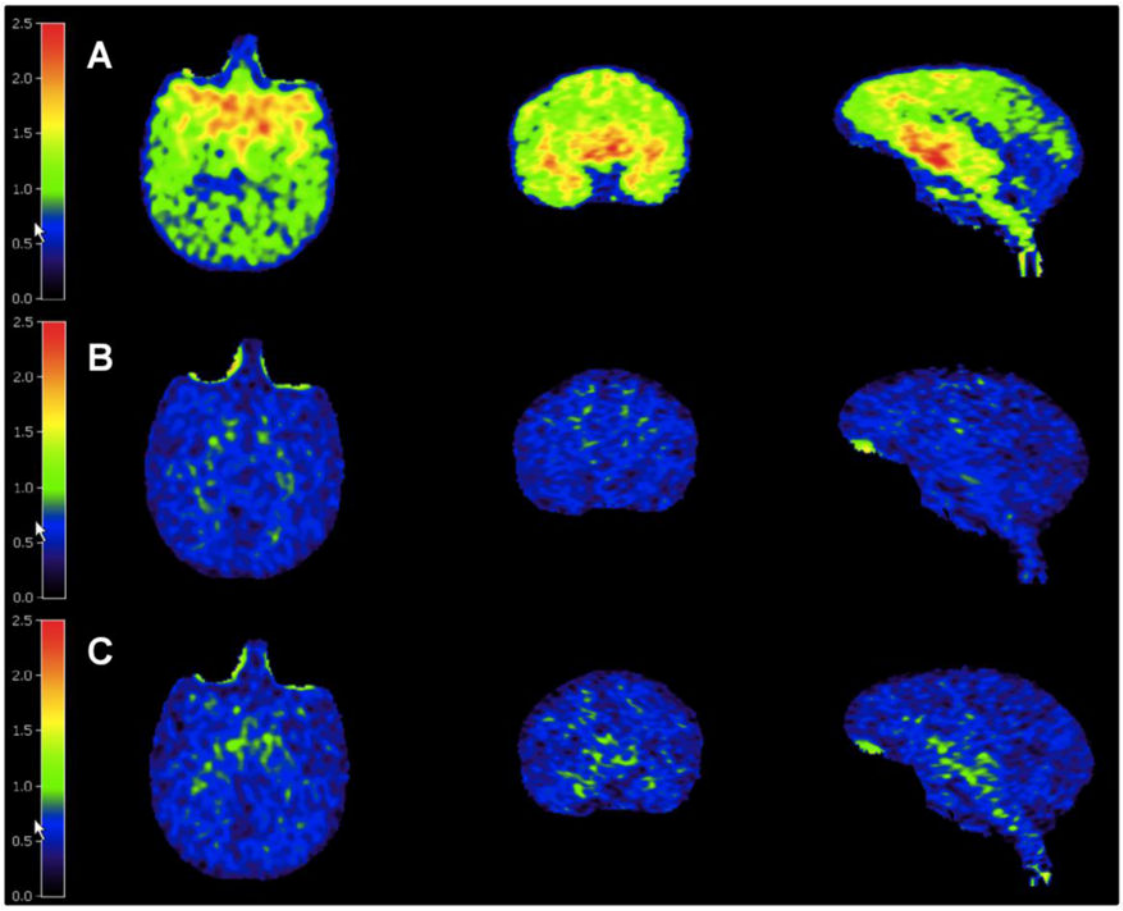

Figure 6.

PET images of ^{11}C-LY2459989 in transaxial (left), coronal (middle) and saggital (right n) views from a baseline scan (A), and blocking scans with 1 mg/kg of naloxone (B) or 0.3 mg/kg of LY2456302 (C). Images are summed from 30–45 min following ^{11}C-LY2459989 injection and presented in standard uptake value (SUV) unit.

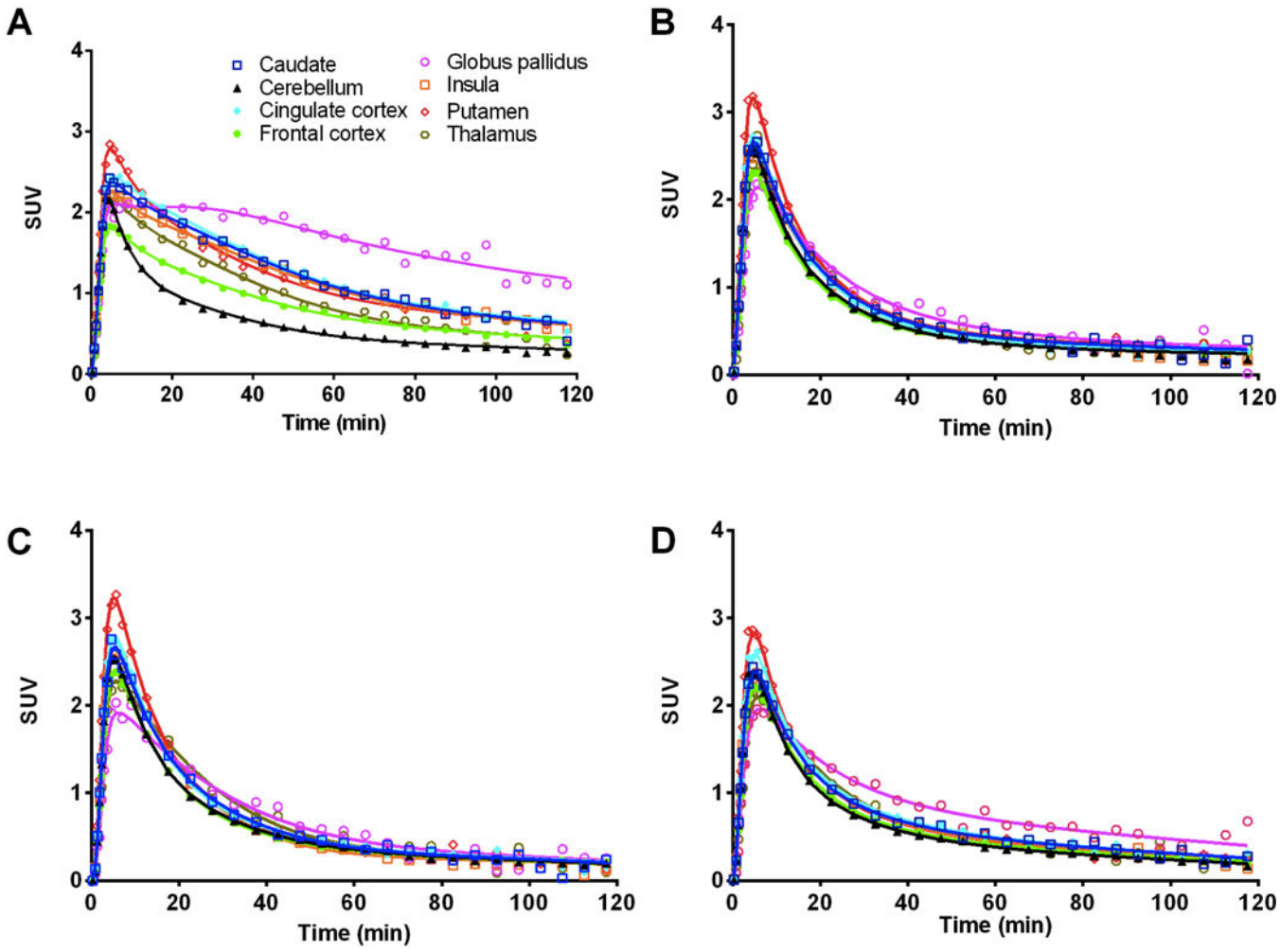

Figure 7.

Time-activity curves in selected brain regions from a ^{11}C-LY2459989 baseline scan (A), and blocking scans after naloxone (B), 0.3 mg/kg of LY2456302 (C), or 36 μg/kg of LY2459989 (D).

Table 1

Regional V_T and BP_{ND} values of ^{11}C-LY2459989 under different conditions[1]

Condition	Blocking Drug Dose (mg/kg)	Globus pallidus	Caudate	Putamen	Cingulate cortex	Insula	Frontal cortex	Temporal cortex	Thalamus	Cerebellum
		V_T (mL·cm^{-3})								
Baseline (n = 6)	–	12.7 ± 1.6	8.2 ± 1.4	8.1 ± 1.2	9.6 ± 2.0	8.4 ± 1.3	6.4 ± 1.0	6.1 ± 0.8	6.0 ± 0.9	4.0 ± 0.6
Naloxone (n = 2)	1.0	5.2 ± 0.6	4.9 ± 0.6	5.3 ± 0.8	4.9 ± 1.0	4.6 ± 0.7	4.4 ± 0.8	4.1 ± 0.5	4.8 ± 0.8	4.3 ± 0.6
LY2456302 (n = 1)	0.03	5.2	4.4	4.2	4.9	4.2	3.7	3.5	4.3	3.2
LY2456302 (n = 1)	0.3	4.2	4.2	4.4	4.2	3.8	3.7	3.7	4.2	3.8
LY2459989 (n = 2)	0.036	6.5 ± 2.1	5.3 ± 1.3	5.0 ± 0.8	5.6 ± 1.6	5.1 ± 1.3	4.5 ± 0.9	4.3 ± 0.6	4.9 ± 0.8	3.9 ± 0.1
^{11}C–LY2795050 baseline (n = 4)[2]		5.2 ± 1.4	3.0 ± 1.4	4.2 ± 0.5	3.7 ± 1.4	3.4 ± 1.0	3.0 ± 1.1	2.8 ± 0.9	–	2.4 ± 0.6
		BP_{ND}								
Baseline (n = 6)	–	2.18 ± 0.23	1.04 ± 0.13	1.03 ± 0.15	1.39 ± 0.25	1.08 ± 0.09	0.59 ± 0.09	0.51 ± 0.08	0.50 ± 0.11	–
Naloxone (n = 2)	1.0	0.20 ± 0.04	0.13 ± 0.02	0.23 ± 0.00	0.14 ± 0.07	0.07 ± 0.01	0.02 ± 0.03	–0.03 ± 0.02	0.10 ± 0.03	–
LY2456302 (n = 1)	0.03	0.64	0.37	0.32	0.53	0.31	0.15	0.09	0.34	–
LY2456302 (n = 1)	0.3	0.09	0.10	0.16	0.11	0.01	–0.02	–0.04	0.12	–
LY2459989 (n = 2)	0.036	0.67 ± 0.22	0.36 ± 0.25	0.30 ± 0.19	0.44 ± 0.30	0.31 ± 0.23	0.16 ± 0.17	0.10 ± 0.11	0.25 ± 0.20	–
^{11}C–LY2795050 baseline (n = 4)[2]		0.97 ± 0.10	0.32 ± 0.26	0.66 ± 0.25	0.63 ± 0.21	0.39 ± 0.17	0.30 ± 0.16	0.15 ± 0.12	–	–

[1] Mean ± SD, where applicable;

[2] Taken from reference (29).